University of Sistan and Baluchestan

Chemical Process Design

Available online at http://cpd.usb.ac.ir/



Thermal Performance Analysis of a Moving Trapezoidal Fin with Temperature-Dependent Variable Thermal Properties Using the Homotopy Perturbation Method

Maryam Khalili Fard[1], Ali Hatami[2]✉, Faramarz Sarhaddi[3]

[1] Faculty of Mathematics, University of Sistan and Baluchestan, Zahedan, Iran. Email: mkhalili.math@pgs.usb.ac.ir
[2] Corresponding Author, Faculty of Mathematics, University of Sistan and Baluchestan, Zahedan, Iran. Email: ahatami@math.usb.ac.ir
[3] Department of Mechanical Engineering, University of Sistan and Baluchestan, Zahedan, Iran. Email: fsarhaddi@eng.usb.ac.ir

ARTICLE INFO

Article type:
Research Article

Article history:
Received: 2026-07-08
Received in revised form: 2026-09-18
Accepted: 2026-09-24
Available online: 2026-09-24

Keywords: *Moving trapezoidal fin; temperature-dependent thermal properties; nonlinear ordinary differential equation; Homotopy Perturbation Method*

ABSTRACT

In the present study, the thermal performance of a moving trapezoidal heat fin featuring temperature-dependent thermophysical properties has been evaluated. The governing equation for the temperature distribution of the fin was formulated for two cases: linear and nonlinear thermal conductivity. The governing equation, being a nonlinear ordinary differential equation (ODE), was solved using the Homotopy Perturbation Method (HPM). The results obtained from HPM show good agreement with numerical results from previous studies. Finally, the effects of design and physical parameters on the dimensionless temperature distribution and fin efficiency were investigated. It was found that increasing the fin taper ratio, convection-conduction parameter, temperature ratio parameter, and radiation-conduction parameter leads to a decrease in the dimensionless temperature of the fin. Conversely, increasing the Péclet number and heat source parameter results in an increase in the dimensionless temperature. Moreover, increasing the aforementioned parameters leads to a reduction in fin efficiency. The dimensionless temperature and fin efficiency for the case of linear thermal conductivity are higher than those for nonlinear thermal conductivity.

Cite this article: Khalili Fard, M., Hatami, A., Sarhaddi, F., (2027), Thermal Performance Analysis of a Moving Trapezoidal Fin with Temperature-Dependent Variable Thermal Properties Using the Homotopy Perturbation Method, *Chemical Process Design*, 6(1), 1-14. http//doi.org/10.22111/cpd.2026.56166.1097

© The Author(s).
DOI: http//doi.org/10.22111/cpd.2026.56166.1097

Publisher: University of Sistan and Baluchestan.

ARTICLE IN PRESS

1. Introduction

A thermal fin is a structural component characterized by its relatively small thickness in comparison to its length, and a minimal cross-sectional area relative to its lateral surface. When attached to thermal systems, fins enhance heat transfer by increasing the effective surface area available for dissipation. They are extensively utilized in various

industrial applications such as electronic cooling systems, heat exchangers, and radiators. To maximize thermal performance, fins are typically fabricated from materials with high thermal conductivity, such as copper or aluminum, which facilitate efficient heat conduction from the source to the surroundings. The efficiency and effectiveness of a fin are governed by several design factors, including its geometry, dimensions, and material composition. Additionally, depending on the operational context, fins may be either stationary or moving. With the rapid advancement of cooling technologies and the increasing demand for high-efficiency thermal management systems, the investigation and optimization of fin designs remain a critical area of research. Numerous theoretical and experimental studies have been conducted to evaluate the performance of various fin configurations under different thermal conditions.

In this research, various analytical, semi-analytical, and numerical methods have been employed to solve the governing equations of heat transfer in fins. The Differential Transform Method (DTM) and its modified versions, such as the DTM-Padé technique, provide the capability to derive series solutions and extend the domain of validity; however, the accuracy of these solutions remains highly dependent on the number of series terms and the implementation of the Padé approximant. Furthermore, the Optimized Adomian Decomposition Method (OADM) is well-suited for solving nonlinear equations, offering an approximate solution without the need for direct linearization. Nevertheless, the computation of higher-order decomposition terms can be algebraically intensive for problems involving complex nonlinearities. The Finite Difference Method (FDM) is a reliable numerical approach for solving heat-transfer problems; however, it depends on domain discretization and appropriate grid selection. For more complex problems, this dependence may lead to increased computational cost and the need to perform a grid-independence (mesh-convergence) study. The Spline Collocation Method (SCM) also offers strong capability for solving nonlinear differential equations; nevertheless, the accuracy of the resulting solution depends on the choice of spline function, the number and distribution of collocation points, and the adopted domain-discretization strategy. In this context, the Homotopy Perturbation Method (HPM), due to its relatively simple solution procedure and its ability to transform the nonlinear governing equation into a sequence of simpler, controllable subproblems, has been proposed as a primary candidate for analyzing nonlinear heat transfer in fins.

In the following, a brief review of selected related studies is presented.

In 2012, Torabi et al. conducted an evaluation of the thermal performance of a longitudinal fin with constant cross-section, subject to a steady fluid velocity and temperature-dependent thermal conductivity [1]. The fin operated under simultaneous convection and radiation heat transfer conditions. The governing heat equation was solved through the application of the Differential Transformation Method (DTM), and the researchers highlighted the efficiency of DTM in solving nonlinear thermal problems with a reasonable computational cost and high accuracy.

Sun and Xu (2015) examined the thermal characteristics of a moving longitudinal fin with a variable cross-sectional area subjected to the influence of combined convective and radiative heat transfer [2]. The thermophysical properties—including thermal conductivity, convective heat transfer coefficient, and radiative emissivity—were considered to be dependent on temperature. The nonlinear governing equation was solved using the Spectral Collocation Method (SCM). Their results revealed that SCM not only provides faster convergence but also yields higher accuracy when compared to traditional numerical methods such as the Finite Volume Method (FVM), Finite Difference Method (FDM), and Finite Element Method (FEM).

Roy and Mallick (2016) performed a detailed thermal analysis of a stationary straight rectangular fin exposed to combined convective–radiative heat transfer conditions [3]. In their formulation, thermal conductivity and emissivity

ARTICLE IN PRESS

were modeled as functions of temperature, whereas the convective heat transfer coefficient was treated as constant. To address the governing problem, the Homotopy Perturbation Method (HPM) was employed to solve the associated nonlinear ordinary differential equation. Their findings confirmed that HPM delivers accurate and efficient results, outperforming several classical approaches reported in the existing literature.

Sobamowo (2017) carried out a thermal analysis of a longitudinal fin with constant cross-section subjected to forced convective heat transfer alongside an internal heat source [4]. In his model, both the temperature-sensitive thermal conductivity and the temperature-dependent internal heat generation were considered, while the convective heat transfer coefficient was taken as a fixed value. The nonlinear ODE governing the system was handled through the Finite Difference Method (FDM).

Patel and Meher (2017) conducted a thermal analysis of a porous fin with constant cross-section under the influence of a magnetic field [5]. The fin was exposed to combined convection–radiation heat transfer, and all thermophysical properties were considered constant. They employed the Adomian Decomposition Sumudu Transform Method (ADSTM) to solve the governing equation.

Oguntala et al. (2019) performed a transient analysis to optimize the thermal performance of a porous rectangular fin subjected to a magnetic field [6]. The fin was exposed to combined convection–radiation heat transfer, and all thermophysical properties were considered temperature-dependent. A nonlinear partial differential equation (PDE) was derived as the governing model and solved using the Finite Volume Method (FVM).

Das and Kundu (2020) conducted a detailed thermal investigation of a porous rectangular fin under the influence of a magnetic field [7]. The fin was exposed to simultaneous convection and radiation mechanisms, and all physical properties were assumed to be constant. The governing nonlinear ordinary differential equation was numerically integrated via a fifth-order Runge–Kutta scheme.

Jayaprakash et al. (2021) obtained the thermal profile of a moving trapezoidal fin subject to an internal heat source [8]. The fin was exposed to simultaneous convection and radiation modes of heat transfer, and all physical properties, as well as the volumetric heat generation term, were considered to be dependent on temperature. The governing temperature distribution equation was formulated as a nonlinear ordinary differential equation (ODE), which was solved using the Differential Transformation technique coupled with Padé approximation (DTM–Padé). Their results demonstrated that the DTM–Padé approach is a simple and highly effective method for solving nonlinear ODEs.

Ud Din et al. (2022) investigated entropy generation in a moving porous fin with an exponentially varying cross-sectional profile in the presence of an internal heating source [9]. The fin was subjected to combined convection–radiation heat transfer. The thermal conductivity was treated as a temperature-dependent property, while other thermophysical properties and the internal heat generation were considered constant. The governing equation was formulated as a nonlinear ordinary differential equation of the second order and was addressed using the shooting technique. From the perspective of entropy minimization, they compared the exponential-profile porous fin with a rectangular porous fin and concluded that the rectangular configuration offers superior thermal performance.

Xu and Hashemi (2023) analyzed the heat transfer behavior of a moving rectangular porous structure under an internal heat source [10]. The fin was subjected to a magnetic field and experienced combined convection–radiation heat transfer to the surrounding environment. All thermophysical parameters, as well as the internal heat generation, were treated as constant. The governing equation for the temperature distribution in the fin was formulated as a second-order

ARTICLE IN PRESS

ordinary differential equation (ODE), which was computed through the Nucci reduction method. The Nucci method provides a closed-form solution for the temperature distribution within the fin.

Riasat et al. (2024) performed a transient thermal analysis of an inclined porous fin with a variable cross section in the presence of an internal heat source [11]. The fin was subjected to combined convective–radiative heat transfer. The internal heat generation was modeled as temperature dependent, while all thermophysical properties were assumed to be constant. The resulting nonlinear partial differential equation (PDE) governing the temperature distribution was solved using the NDSolve command in Mathematica.

Pavithra and Gireesha (2024) analyzed the heat transfer characteristics of a slanted moving porous rectangular fin exposed to a nanofluid flow [12]. The fin was exposed to combined convection–radiation heat transfer, and water condensation also took place inside the fin structure. The convective heat transfer coefficient was considered to be temperature-dependent, while all other thermophysical properties were assumed constant. They employed the Adomian Decomposition Sumudu Transform Method (ADSTM) to solve the nonlinear ordinary differential equation governing the fin's temperature distribution. Their findings demonstrated that the ADSTM provides high accuracy and reliable convergence.

Pavan Kumar et al. (2025) performed a transient thermal analysis of a porous rectangular fin under the influence of moist airflow [13]. The fin was exposed to combined convection–radiation heat transfer. Both the temperature-dependent convective coefficient and relative humidity were considered temperature-dependent, while all other thermophysical properties were assumed to be constant. The governing nonlinear partial differential equation (PDE) was solved numerically through the Finite Difference Method (FDM), and the results were evaluated against those obtained using the Homotopy Analysis Method (HAM). Their findings indicated that the FDM has high capability and reliability in predicting the complex dynamic behavior and coupled heat and mass transfer in the fin.

Ahmad et al. (2025) developed an artificial deep learning–based neural model to predict the heat transfer characteristics of a moving porous triangular fin [14]. The fin was exposed to combined convection–radiation heat transfer, while all thermophysical properties were considered constant. In the design and development of the neural network, the Levenberg–Marquardt backpropagation (LMB) algorithm was employed. Their results demonstrated that the LMB-based neural network predicts the fin's thermal behavior with very high accuracy.

Singh et al. (2025) performed a thermal analysis of a saturated porous hemispherical fin [15]. The fin was exposed to convective modes of heat exchange, where both the convection coefficient and ambient relative humidity were considered temperature-dependent, while all other thermophysical properties were assumed constant. The governing nonlinear ODE describing the fin's temperature field was handled through the Legendre Wavelet Collocation Method (LWCM). Their findings confirmed that LWCM is an efficient and powerful technique for obtaining analytical solutions to heat-transfer phenomena in porous structures.

A review of previous studies reveals that the thermal behavior of moving trapezoidal fins—considering temperature-dependent thermal conductivity and convective heat transfer coefficients—has been solved using various semi-analytical methods. However, in these studies, the radiative emissivity has typically been assumed to be constant, and the effect of its temperature-dependent variations on the thermal performance of the fin has not been investigated. In the present study, in addition to other temperature-dependent heat transfer parameters, the radiative emissivity is also considered as a function of temperature. The resulting nonlinear governing equation is solved using the Homotopy Perturbation Method (HPM). The primary innovation of this research lies in the development of a heat transfer model for moving trapezoidal fins by incorporating temperature-dependent emissivity and providing an HPM-based semi-analytical solution for this nonlinear problem. The HPM has been selected for the current problem due to its

ARTICLE IN PRESS

relatively simple solution procedure and its capability to transform the nonlinear governing equation into a sequence of solvable successive equations. In this method, by utilizing the homotopy expansion, the successive terms of the solution are obtained systematically, and the approximation accuracy can be controlled by increasing the number of terms.

2. Problem Formulation

The present study investigates heat transfer in a moving trapezoidal fin with a length L, a base thickness of $2t_b$ and a width W, as illustrated in Fig. 1.

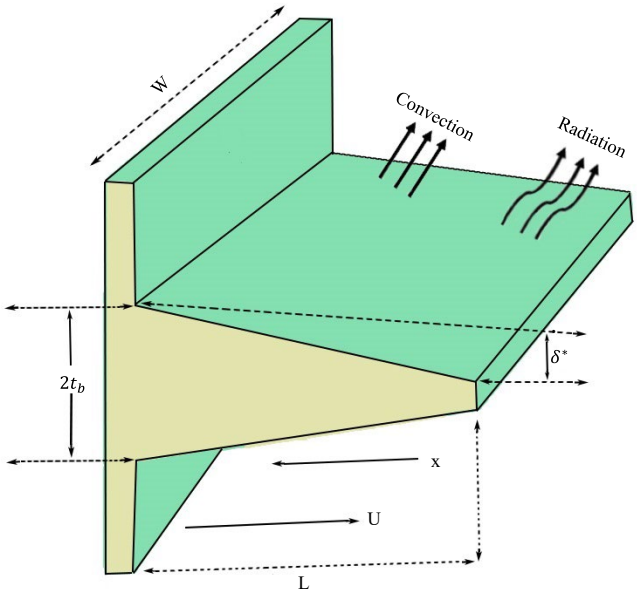


Fig. 1. Moving trapezoidal fin.

According to Fig. 1, heat enters the fin from its base at temperature T_b and is transferred from the lateral surface of the fin to the surrounding environment at temperature T_a via both convection and radiation. The fin moves with a constant velocity U in the longitudinal direction. Additionally, the tip of the fin is assumed to be insulated. The energy equation governing the temperature distribution in the moving trapezoidal fin is expressed as follows [16]:

$$\frac{d}{dx}\left[k^*(T)t(x)\frac{dT}{dx}\right]+\rho c_\rho t(x)U\frac{dT}{dx}+q(T)t(x)=h(T)(T-T_a)+\sigma\varepsilon(T)\left(T^4-T_a^4\right). \quad (1)$$

The fin thickness along its length is considered as a function of the spatial coordinate x and can be expressed as follows [8]:

$$t(x)=\left(t_b+\delta^*\left[\left(\frac{x}{L}\right)-1\right]\right).$$

Here, $\delta^*$is a geometric parameter that defines the thickness of the fin at its tip.

By substituting $t(x)$into Eq. (1), we obtain:

$$\frac{d}{dx}\left[k^*(T)\left(t_b+\delta^*\left[\left(\frac{x}{L}\right)-1\right]\right)\frac{dT}{dx}\right]-h(T)(T-T_a)-\sigma\varepsilon(T)\left(T^4-T_a^4\right) \quad (2)$$

ARTICLE PROCESS

$$+\rho c_{\rho}\left(t_b+\delta^*\left[\left(\frac{x}{L}\right)-1\right]\right)U\frac{dT}{dx}+q\left(T\right)\left(t_b+\delta^*\left[\left(\frac{x}{L}\right)-1\right]\right)=0\ .$$

The heat source parameter q varies linearly with temperature and is expressed as follows [8]:

$$q\left(T\right)=q_0[1+\nu\left(T-T_a\right)]. \tag{3}$$

Furthermore, the parameter q_0 represents the intensity of the heat source, and ν denotes the rate of variation of the heat source with respect to the ambient temperature.

The boundary conditions of the problem are defined as follows [17, 18]:

$$T\left(L\right)=T_b,$$
$$\frac{dT\left(0\right)}{dx}=0. \tag{4}$$

To perform the nondimensionalization process of the governing equation and the boundary conditions, the dimensionless parameters are defined as follows [8]:

$$X=\frac{x}{L},\ \theta=\frac{T-T_a}{T_b-T_a},$$
$$Nc=\frac{h_bL^2}{\kappa_at_b},\ Pe=\frac{\rho C_pLU}{\kappa_a},\ Nr=\frac{\sigma\varepsilon_sL^2}{\kappa_at_b}\left(T_b-T_a\right)^3,\ Nt=\frac{T_a}{T_b-T_a} \tag{5}$$
$$Q=\frac{q_0L^2}{\kappa_a\left(T_b-T_a\right)},\ C=\frac{\delta^*}{t_b},\ \beta=\kappa\left(T_b-T_a\right),\gamma=\nu\left(T_b-T_a\right),\alpha=\varepsilon^*\left(T_b-T_a\right).$$

The thermal conductivity coefficient can be either a linear or a nonlinear function of temperature. The governing equation for the temperature distribution in the fin is presented below for the temperature distribution in the fin is presented for both linear and nonlinear thermal conductivity cases [8]:

2.1. *Case 1: Linear Thermal Conductivity*

Here, the parameters $k^*\left(T\right)$ and $\varepsilon\left(T\right)$ are treated as temperature-dependent linear functions, whereas the parameter $h(T)$ is presumed to follow a nonlinear dependence on temperature [8, 19].

$$k^*\left(T\right)=\kappa_a\left[1+\kappa\left(T-T_a\right)\right],\ h\left(T\right)=h_b\left(\frac{T-T_a}{T_b-T_a}\right)^n,\ \varepsilon\left(T\right)=\varepsilon_s\left[1+\varepsilon^*\left(T-T_a\right)\right]. \tag{6}$$

ARTICLE IN PRESS

Here, the parameters κ and ε^* represent the temperature dependency coefficients for thermal conductivity and emissivity, respectively, and n is the exponent in the variable convective heat transfer coefficient. By substituting Eqs. (3), (5) and (6) into Eq. (2), the dimensionless form of the ordinary differential equation governing the temperature distribution of the fin with linearly varying thermal conductivity is obtained as follows:

$$\frac{d}{dX}\left[(1+\beta\theta)(1+C(X-1))\frac{d\theta}{dX}\right]-Nc\,\theta^{n+1}-Nr\left[(1+\alpha\theta)\left((\theta+Nt)^4-Nt^4\right)\right]$$
$$+Pe\left[1+C(X-1)\right]\frac{d\theta}{dX}+Q\left[1+C(X-1)\right]\left[1+\gamma\theta\right]=0. \quad (7)$$

2.2. *Case 2: Nonlinear Thermal Conductivity*

Here, the parameters $k^*(T)$and $h(T)$ are considered as nonlinear functions of temperature, while the parameter $\varepsilon(T)$ is assumed to vary linearly with temperature [8, 19].

$$k^*(T)=\kappa_a\left[\frac{T-T_a}{T_b-T_a}\right]^m,\ h(T)=h_b\left[\frac{T-T_a}{T_b-T_a}\right]^n,\ \varepsilon(T)=\varepsilon_s\left[1+\varepsilon^*(T-T_a)\right]. \quad (8)$$

Here, the parameters κ_a, h_b, and ε_s represent the thermal conductivity, convective heat-transfer coefficient and radiative heat-transfer coefficient at the ambient temperature T_a, respectively. The parameter m denotes the coefficient of temperature-dependent thermal conductivity.

By substituting Eqs. (3), (5) and (8) into Eq. (2), the dimensionless form of the ordinary differential equation governing the temperature distribution of the moving trapezoidal fin is obtained as follows:

$$m\theta^{m-1}\left[1+C(X-1)\right]\left(\frac{d\theta}{dX}\right)^2+\theta^m C\frac{d\theta}{dX}+\theta^m\left[1+C(X-1)\right]\frac{d^2\theta}{dX^2}-Nc\,\theta^{n+1}$$
$$-Nr\left[(1+\alpha\theta)((\theta+Nt)^4-Nt^4)\right]+Pe\left[1+C(X-1)\right]\frac{d\theta}{dX}+Q\left[1+C(X-1)\right]\left[1+\gamma\theta\right]=0. \quad (9)$$

Similarly, the dimensionless boundary conditions corresponding to Eqs. (7) and (9) are obtained as follows:

$$\theta(1)=1,$$
$$\frac{d\theta(0)}{dX}=0. \quad (10)$$

According to Eqs. (7) and (9), the parameters affecting the fin dimensionless temperature distribution include the thermal conductivity parameter (β), the Péclet number (Pe), the radiation–conduction parameter (Nr), the convection–conduction parameter (Nc), the convective heat transfer coefficient parameter (n), the fin taper ratio (C), the temperature ratio parameter (Nt), the internal heat generation parameter (Q), the temperature-dependence parameter of

ARTICLE IN PRESS

emissivity (α), the temperature-dependence parameter of the heat source (γ), and the variable thermal conductivity heat-transfer parameter (m).

3. Fin efficiency

Fin efficiency is defined as the ratio of the heat carried away by the fin to the amount of heat that would be dissipated from the base surface in the absence of the fin [17, 19]:

Fin efficiency for the case of linear thermal conductivity:

$$\eta = \frac{[1+\beta\theta(1)]\dfrac{d\theta}{dX}}{Nc + Nr[1+\alpha][(1+NT)^4 - Nt^4]}. \tag{11}$$

Fin efficiency in the case of a nonlinear thermal conductivity:

$$\eta = \frac{(\theta(1))^m \dfrac{d\theta}{dX}}{Nc + Nr[1+\alpha][(1+NT)^4 - Nt^4]}. \tag{12}$$

From a theoretical standpoint, the maximum heat transfer from the fin occurs when the entire fin is maintained at the base temperature. Under this ideal condition, the maximum heat transfer consists of both convective and radiative components. Therefore, the denominator of the fin efficiency expressions includes the combined contributions of convective and radiative heat transfer evaluated at the base temperature.

4. Homotopy Perturbation Method (HPM)

The Homotopy Perturbation Method (HPM) is an analytical approach first introduced by He in 1995 and later extended by him in 2000 [20, 21]. This method is effectively applied to solve boundary value problems that may be linear or nonlinear, homogeneous or nonhomogeneous.

The Homotopy Perturbation Method (HPM) facilitates obtaining an approximate solution in the form of a series by integrating the concepts of homotopy and perturbation, without the necessity of assuming a small parameter in the governing equation. Computationally, the structure of HPM is relatively straightforward for solving various nonlinear problems and, unlike the Homotopy Analysis Method (HAM), it typically does not require the determination of an additional convergence-control parameter. Furthermore, similar to the Adomian Decomposition Method (ADM), the solution is derived as a series expansion; however, the framework for generating the series terms differs between the two methods. In many problems, a high-quality approximation of the exact solution can be achieved using only a limited number of HPM series terms.

To demonstrate the idea behind homotopy perturbation, examine the following general form of a nonlinear ordinary differential equation as described in [20]:

$$A^*(u) - f(r) = 0, \quad r \epsilon \Omega \tag{13}$$

ARTICLE IN PRESS

With the boundary conditions:

$$B^*(u, \frac{\partial u}{\partial X}) = 0, \qquad r \in \Gamma \tag{14}$$

Here, $A^*(u)$ denotes the differential operator, B^* is the boundary operator, $f(r)$ is a known analytical function, and r belongs to the domain Ω. The operator $A^*(u)$ can generally be decomposed into two components: a linear operator $L^*(u)$ and a nonlinear operator $N^*(u)$.

Accordingly, the differential Eq. (11) can be rewritten as:

$$L^*(u) + N^*(u) - f(r) = 0 \tag{15}$$

In the first step of the Homotopy Perturbation Method (HPM), a homotopy $\theta(r,p): \Omega \times [0,1] \to R$ is constructed to satisfy the following relation:

$$H(\theta, p) = (1-p)\left[L^*(\theta) - L^*(u_0)\right] + p\left[L^*(\theta) + N^*(\theta) - f(r)\right] = 0 \tag{16}$$

Eq. (16) can be rewritten as follows:

$$H(\theta, p) = L^*(\theta) - L^*(u_0) + pL^*(u_0) + p\left[N^*(\theta) - f(r)\right] = 0 \tag{17}$$

Here, u_0 is the initial guess of the solution to Eq. (13), which satisfies the boundary conditions in Eq. (14), and $p \epsilon [0, 1]$ is referred to as the homotopy parameter.

Therefore, when $p = 0$, we obtain:

$$H(\theta, 0) = \left[L^*(\theta) - L^*(u_0)\right] = 0 \tag{18}$$

And when $p = 1$, we have:

$$H(\theta, 1) = \left[L^*(\theta) + N^*(\theta) - f(r)\right] = 0 \tag{19}$$

It is assumed that the solution of Eq. (13) can be expressed as a power series in terms of p, in the following form:

$$\theta = \theta_0 + p\theta_1 + p^2\theta_2 + p^3\theta_3 + p^4\theta_4 + \ldots \tag{20}$$

By substituting $p = 1$ into Eq. (20), the approximate solution of Eq. (13) is obtained as follows:

$$u = \theta_0 + \theta_1 + \theta_2 + \theta_3 + \theta_4 + \ldots \tag{21}$$

ARTICLE IN PRESS

5. Solution Of the Governing Equation Using the Homotopy Perturbation Method

5.1. *Case 1: Linear Thermal Conductivity*

To apply the Homotopy Perturbation Method, the governing Eq. (7) can be rewritten using Eq. (17) as follows:

$$\begin{aligned} H(\theta,p) &= L^*(\theta) - L^*(u_0) + pL^*(u_0) + p[\left((1+\beta\theta)\left(1+C(X-1)\right)\right)\frac{d^2\theta}{dX^2} \\ &+\beta\left(1+C(X-1)\right)\left(\frac{d\theta}{dX}\right)^2 + Pe\left(1+C(X-1)\right)\frac{d\theta}{dX} - Nc\theta^{n+1} \\ &-Nr\left((1+\alpha\theta)\left((\theta+Nt)^4 - Nt^4\right)\right) + Q\left(1+C(X-1)\right)(1+\gamma\theta) = 0. \end{aligned} \tag{22}$$

Here, $L^* = \frac{d^2}{dX^2}$. By substituting Eq. (20) into Eq. (22) and separating the different powers of p, the following system of equations is obtained:

$$p^0 : \frac{d^2\theta_0}{dX^2} - \frac{d^2u_0}{dX^2} = 0 \ . \tag{23}$$

According to the boundary conditions defined in Eq. (10), it is evident that the solution of the governing equation does not yield a physically meaningful result. Therefore, in order to obtain a physically realistic prediction, the dimensionless temperature at the fin tip (i.e., at $X=0$) is assumed to be a constant value K. Hence, we have $\theta(0)=K$. Considering the boundary condition $\theta(0)=K$, the value K is treated as an unknown constant and is used as the initial value for constructing the HPM expansion. Since the present problem is a boundary-value problem and the boundary conditions are imposed at both ends of the domain, i.e., $X=0$ and $X=1$, introducing the unknown constant K enables the boundary condition at $X=1$ to be enforced systematically after obtaining the HPM series solution. In this approach, K is not an independent physical parameter; rather, it is determined by applying the boundary condition $\theta(1)=1$ so that both boundary conditions are satisfied simultaneously.

Based on Eq. (20), this leads to $\theta_0(0)=K$, which is considered as the initial approximation for applying the Homotopy Perturbation Method (HPM).

In the following, similarly, for the subsequent orders of p, we have:

$$\begin{aligned} p^1 : &\frac{d^2\theta_1}{dX^2} + \frac{d^2u_0}{dX^2} + [C(X-1)\frac{d^2\theta_0}{dX^2} + C(X-1)\beta\theta_0\frac{d^2\theta_0}{dX^2} + \beta\theta_0\frac{d^2\theta_0}{dX^2} \\ &+\beta\left(1+C(X-1)\right)\left(\frac{d\theta_0}{dX}\right)^2 + C(1+\beta\theta_0)\frac{d\theta_0}{dX} + Pe\left(1+C(X-1)\right)\frac{d\theta_0}{dX} - Nc\theta_0^{n+1} \\ &+Nr(-4Nt^3\theta_0 - 6Nt^2\theta_0^2 - 4Nt^3\alpha\theta_0^2 - 4Nt\theta_0^3 - 6Nt^2\alpha\theta_0^3 - \theta_0^4 - 4Nt\alpha\theta_0^4 - \alpha\theta_0^5) \end{aligned}$$

ARTICLE IN PRESS

$$+Q\left(1+C\left(X-1\right)\right)\left(1+\gamma\theta_0\right)=0, \tag{24}$$

$$\theta_1(0)=0, \qquad \frac{d\theta_1(0)}{dX}=0.$$

and

$$p^2:\frac{d^2\theta_2}{dX^2}+[C\left(X-1\right)\frac{d^2\theta_1}{dX^2}+\left(1+C\left(X-1\right)\right)\beta\theta_0\frac{d^2\theta_1}{dX^2}+\left(1+C\left(X-1\right)\right)\beta\theta_1\frac{d^2\theta_0}{dX^2}$$
$$+C\beta\theta_1\frac{d\theta_0}{dX}+(C+Pe-CPe+CPeX+C\beta\theta_0)\frac{d\theta_1}{dX}+2\left(1+C\left(X-1\right)\right)\beta\theta_0\frac{d\theta_1}{dX}$$
$$-\left(n+1\right)Nc\theta_0{}^n\theta_1+Nr(-(4Nt^3+4Nt^2\left(3+2Nt\alpha\right)\theta_0+6Nt\left(2+3Nt\alpha\right)\theta_0{}^2$$
$$+4\left(1+4Nt\alpha\right)\theta_0{}^3+5\alpha\theta_0{}^4)\theta_1)+Q\left(1+C\left(X-1\right)\right)\gamma\theta_1=0, \tag{25}$$

$$\theta_2(0)=0, \qquad \frac{d\theta_2(0)}{dX}=0.$$

and

$$p^3:\frac{d^2\theta_2}{dX^2}+\ [C\left(X-1\right)\frac{d^2\theta_2}{dX^2}+\left(1+C\left(X-1\right)\right)\beta\theta_0\frac{d^2\theta_2}{dX^2}+\left(1+C\left(X-1\right)\right)\beta\theta_1\frac{d^2\theta_1}{dX^2}$$
$$+\left(1+C\left(X-1\right)\right)\beta\theta_2\frac{d^2\theta_0}{dX^2}+\beta\left(1+C\left(X-1\right)\right)\left(\frac{d\theta_1}{dX}\right)^2$$
$$+\left(C+Pe-CPe+CPeX+C\beta\theta_0+2\left(1+C\left(X-1\right)\right)\beta\frac{d\theta_0}{dX}\right)\frac{d\theta_2}{dX}$$
$$+C\beta\theta_2\frac{d\theta_0}{dX}+C\beta\theta_1\frac{d\theta_1}{dX}-\frac{1}{2}Nc\left(n+1\right)\theta_0{}^{n-1}\left(n\theta_1{}^2+2\theta_0\theta_2\right)$$
$$+Nr(-2\left(Nt+\theta_0\right)^2\left(3+2Nt\alpha+3\lambda+5\alpha\theta_0\right)\theta_1{}^2-(4Nt^3+4Nt^2\left(3+2Nt\alpha\right)\theta_0$$
$$+6Nt(2+3Nt\alpha)\theta_0^2+4(1+4Nt\alpha)\theta_0^3+5\alpha\theta_0^4)\theta_2)+Q(1+3)X-1))\gamma\theta_2]=0,$$

$$\theta_3(0)=0, \quad \frac{d\theta_3(0)}{dX}=0.$$

and

$$p^4:\frac{d^2\theta_4}{dX^2}+[C\left(X-1\right)\frac{d^2\theta_3}{dX^2}+\left(1+C\left(X-1\right)\right)\beta\theta_0\frac{d^2\theta_3}{dX^2}+\left(1+C\left(X-1\right)\right)\beta\theta_1\frac{d^2\theta_2}{dX^2} \tag{26}$$
$$+\left(1+C\left(X-1\right)\right)\beta\theta_2\frac{d^2\theta_1}{dX^2}+\left(1+C\left(X-1\right)\right)\beta\theta_3\frac{d^2\theta_0}{dX^2}$$
$$+\left(C+Pe-CPe+CPeX+C\beta\theta_0+2\left(1+C\left(X-1\right)\right)\beta\theta_0\right)\frac{d\theta_3}{dX}$$

ARTICLE IN PRESS

$$+(\beta\left(C\theta_1+2\left(1+C\left(X-1\right)\right)\frac{d\theta_1}{dX}\right)\frac{d\theta_2}{dX}+C\beta\theta_2\frac{d\theta_1}{dX}+C\beta\theta_3\frac{d\theta_0}{dX}$$

$$-Nc\frac{1}{6}\left(n+1\right)\theta_0^{n-2}\left(\left(n-1\right)n\theta_1^3+6n\theta_0\theta_1\theta_2+6\theta_0^2\theta_3\right)$$

$$+Nr(-2\left(Nt+\theta_0\right)\left(2+3Nt\alpha+5\alpha\theta_0\right)\theta_1^3-4\left(Nt+\theta_0\right)^2\left(3+2Nt\alpha+5\alpha\theta_0\right)\theta_1\theta_2$$

$$-\left(4Nt^3+4Nt^2\left(3+2Nt\alpha\right)\theta_0+6Nt\left(2+3Nt\alpha\right)\theta_0^2+4\left(1+4Nt\alpha\right)\theta_0^3+5\alpha\theta_0^4\right)\theta_3)$$

$$+Q\left(1+C\left(X-1\right)\right)\gamma\theta_3]=0,$$

$$\theta_4\left(0\right)=0,\quad\frac{d\theta_4\left(0\right)}{dX}=0. \tag{27}$$

Next, by solving Eqs. (23)–(27), the quantities θ_0, θ_1, θ_2, θ_3, and θ_4 are obtained. It is evident that including more terms in the expansion would result in higher accuracy. However, in most cases, expansion up to the fourth term provides a sufficiently accurate solution [23]. In the present study, the HPM expansion is carried out up to the fourth-order term, which is adopted as the final approximation.

For instance, for the parameter values $C=0.4$, $Q=0.1$, $n=0, Nc=1$, $\beta=1$, $Nr=1$, $Pe=1$, $\gamma=0.1, Nt=0.1$ and $\alpha=0.1$, and by employing Eq. (20) along with the boundary condition $\theta\left(1\right)=1$, the constant value $K=0.6546767622841139$ is obtained. Consequently, the final approximate solution of the problem, according to Eq. (21), is expressed as follows:

$$\theta\left(X\right)=0.6546767622841139+0.471517304711966X^2$$

$$-0.31170417423545044X^3+0.2171855052464125X^4$$

$$-0.11523648862472903X^5+0.13448793380221225X^6$$

$$-0.06383120437046985X^7+0.013236086592978622X^8$$

$$-0.0003349802569608899X^9+0.000003267035146612228X^{10}$$

$$-1.218522131464267\times10^{-8}X^{11}+1.594414779241918\times10^{-15}X^{12}. \tag{28}$$

5.2. *Case 2: Nonlinear Thermal Conductivity*

To apply the Homotopy Perturbation Method (HPM), using Eq. (17), the governing Eq. (9) can be rewritten as follows:

$$H\left(\theta,p\right)=L^*\left(\theta\right)-L^*\left(u_0\right)+pL^*\left(u_0\right)+p[\left(1+C\left(X-1\right)\right)\frac{d^2\theta}{dX^2}+C\frac{d\theta}{dX}-Nc\theta^{n+1}$$

$$+Pe\left(1+C\left(X-1\right)\right)\frac{d\theta}{dX}-Nr\left(1+\alpha\theta\right)\left(\left(\theta+Nt\right)^4-Nt^4\right))+Q\left(1+C\left(X-1\right)\right)\left(1+\gamma\theta\right)]=0. \tag{29}$$

Here, $L^*=\frac{d^2}{dX^2}$.

By substituting Eq. (20) into Eq. (29) and separating the terms according to the powers of p, the following system of equations is obtained:

ARTICLE IN PRESS

$$p^0 : \frac{d^2\theta_0}{dX^2} - \frac{d^2u_0}{dX^2} = 0. \tag{30}$$

According to the boundary conditions given in Eq. (10), it is evident that the solution of the governing equation lacks physical significance. Therefore, to obtain a physically meaningful solution, the value of θ at the fin tip ($X = 0$) is assumed to be a constant K, that is, $\theta(0) = K$. Consequently, based on Eq. (20), $\theta_0(0) = K$ is considered as the initial value for the HPM.

Similarly, the equations corresponding to the higher-order terms of the parameter p can be obtained as follows:

$$\begin{aligned} p^1 : &\frac{d^2\theta_1}{dX^2} + \frac{d^2u_0}{dX^2} + [C(X-1)\frac{d^2\theta_0}{dX^2} + Pe\frac{d\theta_0}{dX} + C\left(1 + Pe(X-1)\right)\frac{d\theta_0}{dX} \\ &-Nc\theta_0^{n+1} + Nr(-4Nt^3\theta_0 - 2Nt^2(3+2Nt\alpha)\theta_0^2 - 2Nt(2+3Nt\alpha)\theta_0^3 \\ &-(1+4Nt\alpha)\theta_0^4 - \alpha\theta_0^5) + Q\left(1 + C(X-1)\right)(1+\gamma\theta_0)], \\ &\theta_1(0) = 0, \quad \frac{d\theta_1(0)}{dX} = 0. \end{aligned} \tag{31}$$

and

$$\begin{aligned} p^2 : &\frac{d^2\theta_2}{dX^2} + [C(X-1)\frac{d^2\theta_1}{dX^2} + Pe\frac{d\theta_1}{dX} + C\left(1 + Pe(X-1)\right)\frac{d\theta_1}{dX} - (n+1)Nc\theta_0^n\theta_1 \\ &+Nr(4Nt^3(1+4Nt^2(3+2Nt\alpha)\theta_0 + 6Nt(2+3Nt\alpha)\theta_0^2 \\ &+4(1+4Nt\alpha)\theta_0^3 + 5\alpha\theta_0^4)\theta_1 + Q\left(1C(X-1)\right)\gamma\theta_1] = 0, \\ &\theta_2(0) = 0, \quad \frac{d\theta_2(0)}{dX} = 0. \end{aligned} \tag{32}$$

and

$$\begin{aligned} p^3 : &\frac{d^2\theta_2}{dX^2} + [C(X-1)\frac{d^2\theta_2}{dX^2} + Pe\frac{d\theta_2}{dX} + C\left(1 + Pe(X-1)\right)\frac{d\theta_2}{dX} \\ &-\frac{1}{2}Nc(n+1)\theta_0^{n-1}\left(n\theta_1^2 + 2\theta_0\theta_2\right) + Nr(-2(Nt+\theta_0)^2(3+2Nt\alpha+3\lambda+5\alpha\theta_0)\ \theta_1^2) \\ &-(4Nt^3 + 4Nt^2(3+2Nt\alpha+)\theta_0 + 6Nt(2+3Nt\alpha)\theta_0^2 \\ &+4(1+4Nt\alpha)\theta_0^3 + 5\alpha\theta_0^4)\theta_2) + Q\left(1 + C(X-1)\right)\gamma\theta_2] = 0, \\ &\theta_3(0) = 0, \quad \frac{d\theta_3(0)}{dX} = 0, \end{aligned} \tag{33}$$

and

ARTICLE IN PRESS

$$
\begin{aligned}
p^4 :& \frac{d^2\theta_4}{dX^2} + [C\,(X-1)\frac{d^2\theta_3}{dX^2} + Pe\,\frac{d\theta_3}{dX} + C\,(1+Pe\,(X-1))\frac{d\theta_3}{dX} \\
& -\frac{1}{6}Nc\,(n+1)\theta_0^{n-2}\left((n-1)n\theta_1^3 + 6n\theta_0\theta_1\theta_2 + 6\theta_0^2\theta_3\right) \\
& +Nr(-2\left(Nt+\theta_0\right)\left(2+3Nt\alpha+5\alpha\theta_0\right)\theta_1^3) - 4\left(Nt+\theta_0\right)^2(3+2Nt\alpha+5\alpha\theta_0)\;\theta_1\theta_2 \\
& -(4Nt^3 + 4Nt^2\left(3+2Nt\alpha+\right)\theta_0 + 6Nt\left(2+3Nt\alpha\right)\theta_0^2 \\
& +4\left(1+4Nt\alpha\right)\theta_0^3 + 5\alpha\theta_0^4)\theta_3) + Q\left(1+C\,(X-1)\right)\gamma\theta_3] \\
\theta_4(0) = 0\,, \qquad & \frac{d\theta_4(0)}{dX} = 0.
\end{aligned}
\tag{34}
$$

Subsequently, solving Eqs. (30)–(34) yields θ_0, θ_1, θ_2, θ_3, and θ_4. It is evident that expanding the series to include additional terms would yield more accurate results; however, in most cases, an expansion up to four terms is sufficient [23].

As an example, for the parameter values $C=0.4$, $Q=0.1$, $n=0$, $Nc=1$, $\beta=1$, $Nr=1$, $Pe=1$, $\gamma=0.1$, $Nt=0.1$ and $\alpha=0.1$, utilizing Eq. (20) and applying the boundary condition $\theta(1)=1$, the constant $K=0.574498872990640$ is obtained. The final solution to the problem, based on Eq. (21), is expressed as follows:

$$
\begin{aligned}
\theta(X) = {} & 0.5815435748041408 + 0.6059613036173042X^2 \\
& -0.4084654144664860 4X^3 + 0.2899011270867677X^4 \\
& -0.1076018783150423 5X^5 + 0.0509313495821357 8X^6 \\
& -0.0174425242272072 2X^7 + 0.0053457666109166 72X^8 \\
& -0.0001755002063068984X^9 + 0.0000022060805599053 68X^{10} \\
& -1.056678407983622\times10^{-8}X^{11} + 1.583470793087 04\times10^{-15}X^{12}.
\end{aligned}
\tag{35}
$$

6. Validation

For validation purposes, the results obtained from the HPM method in the present study are compared with the DTM results reported in reference [8] and the OADM results presented in reference [22]. The outcomes of this comparison are provided in Table 1. As can be observed, there is a very good agreement between the HPM results of this study and the analytical solutions reported in references [8] and [22].

Table 1. Validation of the results obtained in this study with previous works for the fin tip temperature, in the case where $C = Nt = Q = n = \gamma = \alpha = 0$, $Nr = 0.5$.

Pe	Nc	β	(OADM) [22]	(DTM) [8]	Present result (HPM)	$\lvert OADM - HPM \rvert$	$\lvert DTM - HPM \rvert$
0.25	0.25	0.25	0.8190	0.8193	0.8187	0.0003	0.0006
		0.50	0.8384	0.8388	0.8371	0.0013	0.0017
		0.75	0.8541	0.8544	0.8541	0.0000	0.0003
0.50	0.50	0.25	0.7741	0.7740	0.7736	0.0005	0.0004
		0.50	0.7967	0.7972	0.7944	0.0023	0.0028

ARTICLE IN PRESS

		0.75		0.8153		0.8160		0.8135		0.0018		0.0025

For further validation, the results of the present study using the HPM method are compared with the DTM and RKF-45 results reported in reference [8], as presented in Table 2.

Table 2. Validation of the results obtained in this study with previous works for the fin tip temperature, in the case where $n = \alpha = 0$.

C	Nc	Nr	Nt	Q	γ	Pe	β	DTM [8]	RKF-45 [8]	Preset result (HPM)	$\lvert DTM - HPM \rvert$	$\lvert RKF - HPM \rvert$
0.1	0.5	0.25	0.5	0.3	0.3	0.5	0.1	0.7261	0.7207	0.7207	0.0054	0.0000
0.2								0.7162	0.7085	0.7085	0.0077	0.0000
	0.6							0.6988	0.6910	0.6910	0.0078	0.0000
	0.7							0.6817	0.6739	0.6739	0.0078	0.0000
		0.5						0.6181	0.6109	0.6109	0.0072	0.0000
		0.75						0.5480	0.5395	0.5397	0.0083	0.0002
			0.6					0.5627	0.5548	0.5548	0.0079	0.0002
			0.7					0.5066	0.4983	0.4985	0.0081	0.0002
				0.5				0.6571	0.6525	0.6525	0.0046	0.0000
				0.6				0.6724	0.6728	0.6728	0.0004	0.0000
					0.4			0.6220	0.6144	0.6144	0.0076	0.0000
					0.5			0.6258	0.6180	0.6180	0.0078	0.0000
						0.75		0.6293	0.6207	0.6207	0.0086	0.0000
						1.0		0.6388	0.6303	0.6303	0.0085	0.0000
							0.3	0.6362	0.6317	0.6317	0.0045	0.0000
							0.5	0.6514	0.6505	0.6505	0.0009	0.0000

Furthermore, the HPM results are compared with the numerical RKF-45 results in Table 3. An examination of the corresponding data reveals good agreement between the HPM predictions and the numerical RKF-45 solution. Moreover, the comparison presented in Table 3 at the considered points indicates that the fourth-order expansion provides sufficient accuracy for predicting the fin temperature in the present problem.

Table 3. Validation of the results obtained in this study with the RKF45 numerical values for the dimensionless temperature $\theta(X)$ at selected collocation points, along with the corresponding absolute error, for $C = 0.1, Nc = 0.5, Nr = 0.25, Nt = 0.5, Q = 0.3, \gamma = 0.3, Pe = 0.5, \beta = 0.1, \alpha = 0.1, n = m = 1$.

X	Present result (HPM)	RKF-45	$\lvert RKF - HPM \rvert$
0	0.6984	0.6986	0.0002
0.1	0.7019	0.7021	0.0002
0.2	0.7120	0.7122	0.0002
0.3	0.7281	0.7283	0.0002
0.4	0.7499	0.7501	0.0002
0.5	0.7771	0.7774	0.0003
0.6	0.8098	0.8101	0.0003
0.7	0.8481	0.8484	0.0003
0.8	0.8923	0.8925	0.0002
0.9	0.9427	0.9428	0.0001
1	1.0000	1.0000	0.0000

ARTICLE IN PRESS

7. Results And Discussion

In the present study, the governing equation for the temperature distribution in a trapezoidal fin has been solved using the Homotopy Perturbation Method (HPM). Representative HPM results for various physical parameters are provided in Tables 3 and 4. Table 3 presents the results for the solution of the ordinary differential equation governing the temperature distribution assuming a linear thermal conductivity, while Table 4 corresponds to the results obtained for a nonlinear thermal conductivity. Furthermore, in both tables, the results obtained via HPM are compared with those of the numerical RKF-45 method. An examination of the data in the respective tables reveals a good agreement between the HPM results and those obtained using the RKF-45 numerical technique.

Table 4. Examination of the convergence of the HPM solution with the numerical fin tip temperature results under various physical parameters ($n=1$).

C	Nc	Nr	Nt	Q	γ	Pe	β	α	HPM	RKF-45	$\lvert RKF - HPM \rvert$
0.1	0.5	0.25	0.5	0.3	0.3	0.5	0.1	0.1	0.7290	0.7290	0.0000
0.2									0.7181	0.7180	0.0001
	0.6								0.7169	0.7170	0.0001
	0.7								0.7053	0.7053	0.0000
		0.5							0.6191	0.6191	0.0000
		0.75							0.5476	0.5473	0.0003
			0.6						0.6843	0.6843	0.0000
			0.7						0.6373	0.6373	0.0000
				0.4					0.7527	0.7527	0.0000
				0.5					0.7760	0.7760	0.0000
					0.4				0.7335	0.7335	0.0000
					0.5				0.7380	0.7380	0.0000
						0.75			0.7370	0.7370	0.0000
						1.0			0.7447	0.7443	0.0004
							0.3		0.7462	0.7463	0.0001
							0.5		0.7601	0.7616	0.0015
								0.2	0.7188	0.7188	0.0000
								0.3	0.7092	0.7092	0.0000

ARTICLE IN PRESS

Table 5. Examination of the convergence of the HPM solution with the numerical fin tip temperature results under various physical parameters ($n=m=1$).

C	Nc	Nr	Nt	Q	γ	Pe	α	HPM	RKF-45	|RKF − HPM|
0.1	0.5	0.25	0.5	0.3	0.3	0.5	0.1	0.6984	0.6986	0.0002
0.2								0.6841	0.6855	0.0014
	0.6							0.6843	0.6846	0.0003
	0.7							0.6707	0.6711	0.0004
		0.5						0.5710	0.5717	0.0007
		0.75						0.4857	0.4880	0.0023
			0.6					0.6456	0.6463	0.0007
			0.7					0.5884	0.5904	0.0020
				0.4				0.7277	0.7273	0.0004
				0.5				0.7555	0.7550	0.0005
					0.4			0.7039	0.7040	0.0001
					0.5			0.7093	0.7094	0.0001
						0.75		0.7068	0.7098	0.0030
						1.0		0.7149	0.7202	0.0053
							0.2	0.6871	0.6872	0.0001
							0.3	0.6764	0.6765	0.0001

In this study, the energy equation governing the temperature distribution of a moving trapezoidal fin in the presence of an internal heat source was formulated and solved using the Homotopy Perturbation Method (HPM) for both linear and nonlinear thermal conductivity cases. Subsequently, the effects of various dimensionless design and performance parameters—including thermal conductivity (β), Péclet number (Pe), radiation–conduction parameter (Nr), convection–conduction parameter (Nc), temperature ratio parameter (Nt), heat source parameter (Q), convective heat transfer coefficient parameter (n), and fin taper ratio (C)—on the dimensionless temperature distribution and fin efficiency were investigated.

Fig. 2(a) depicts how the fin aspect ratio (C) influences the dimensionless temperature distribution under linear thermal conductivity. In contrast, Fig. 2(b) shows the effect of the same parameter C on the dimensionless temperature distribution when the thermal conductivity is nonlinear.

ARTICLE IN PRESS

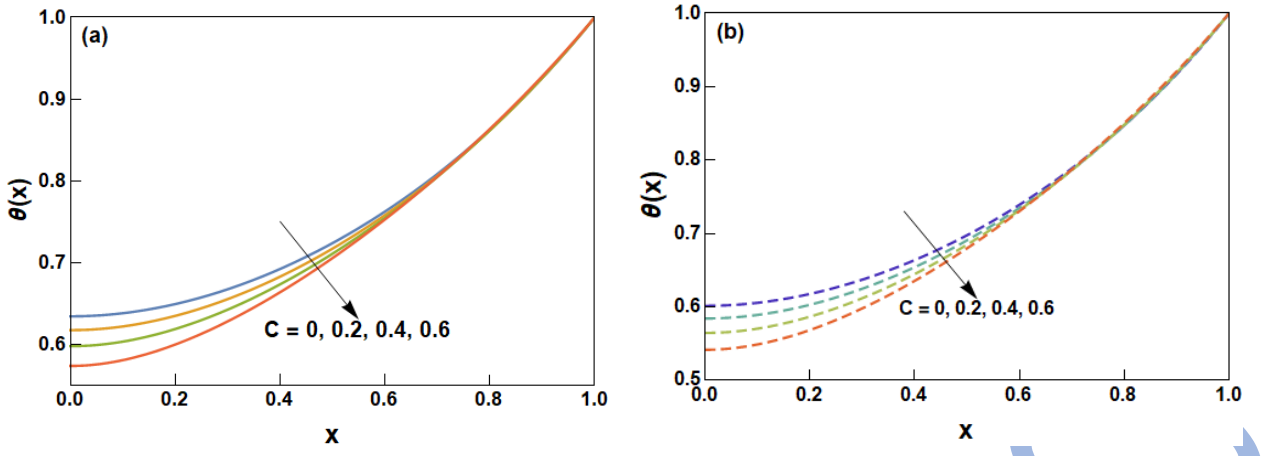


Fig. 2. Investigation of the effect of parameter Con $\theta(X)$ for (a) linear and (b) nonlinear thermal conductivity. (Nc = 1, Nt = 0.1, Nr =1, Pe = 1, Q = 0, $n = 0, \gamma = 0.3,\ \beta = 0.3,\ \alpha = 0.1, m = 0$).

As shown in Fig. 2, the fin dimensionless temperature decreases with increasing fin taper ratio C. For the geometry considered, an increase in Cintensifies the variation in fin thickness along its length and consequently alters the shape of the trapezoidal fin. This geometric modification changes the heat-transfer conditions between the fin surface and the surrounding medium and, under the conditions examined, leads to greater heat dissipation through convection and radiation; as a result, the fin dimensionless temperature decreases.

Figs. 3(a) and 3(b) respectively illustrate how the convection–conduction parameter (Nc) influences the dimensionless temperature distribution of the fin in the cases of linear and nonlinear thermal conductivity.

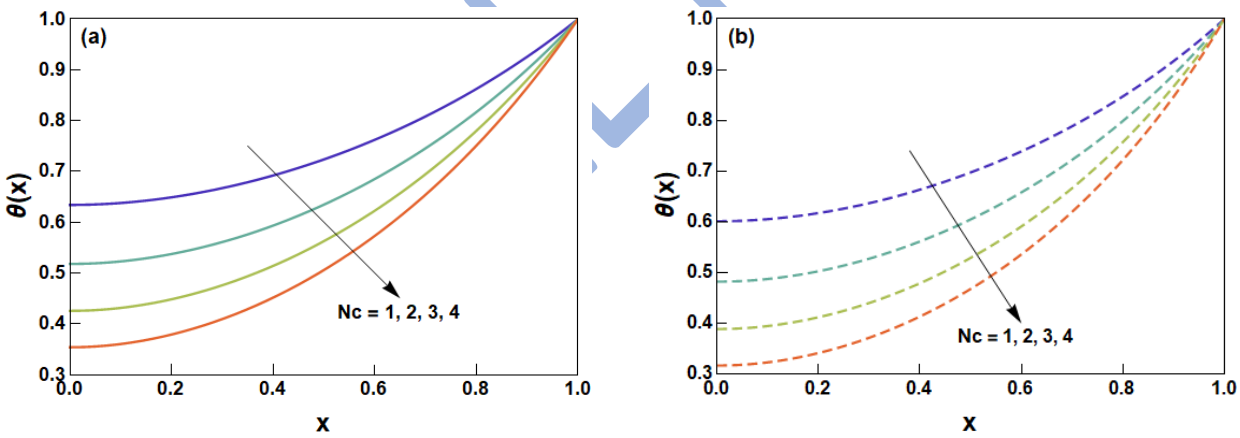


Fig. 3. Investigation of the effect of parameter Nc on $\theta(X)$ for (a) linear and (b) nonlinear thermal conductivity. ($C = 0$, Nt = 0.1, Nr =1, Pe = 1, Q = 0, $n = 0$, $\gamma = 0.3$, $\beta = 0.3$, $\alpha = 0.1$, $m = 0$).

Fig. 3 demonstrates that increasing the convection–conduction parameter (Nc) intensifies the heat removed from the fin's surface. As the rate of thermal dissipation grows, the fin's dimensionless temperature correspondingly declines. The influence of the temperature-ratio parameter (Nt) on the nondimensional temperature field of the fin is depicted in Figs. 4(a) and 4(b). These plots correspond to the linear and nonlinear thermal-conductivity states, respectively.

AI - IN PRESS

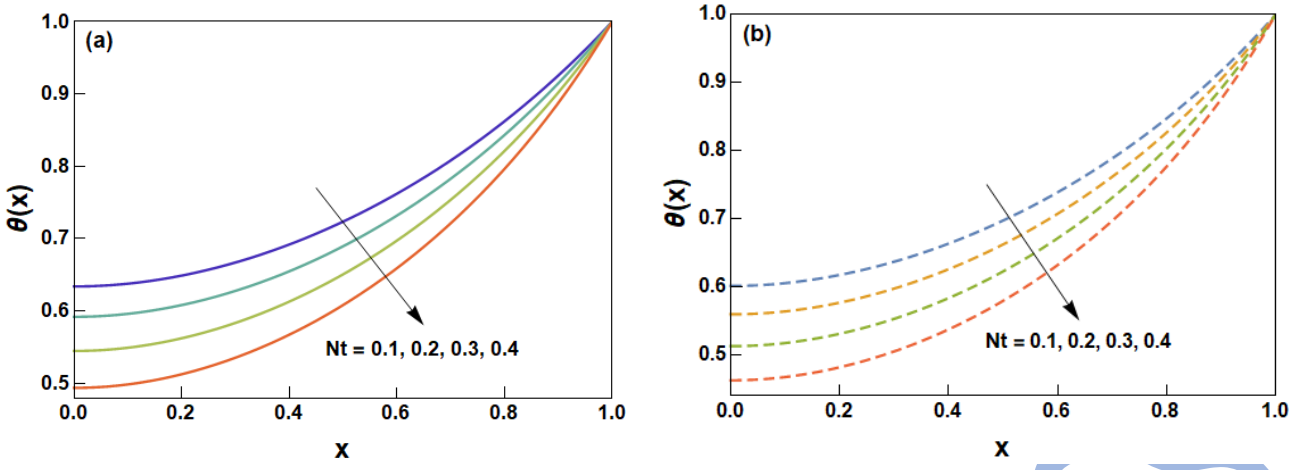


Fig. 4. Investigation of the effect of parameter Nt on $\theta(X)$ for (a) linear and (b) nonlinear thermal conductivity. ($C = 0$, $Nc = 1$, $Nr = 1$, $Pe = 1$, $Q = 0$, $n = 0$, $\gamma = 0.3$, $\beta = 0.3$, $\alpha = 0.1$, $m = 0$).

As illustrated in Fig. 4, an increase in the temperature ratio parameter (Nt) causes a decline in the dimensionless temperature distribution of the fin. Larger values of Nt are associated with a higher convective heat transfer coefficient. As a result, greater convective heat dissipation from the fin occurs, which ultimately lowers the fin's dimensionless temperature.

Fig. 5 presents how the radiation–conduction parameter (Nr) influences the fin's nondimensional temperature behavior.

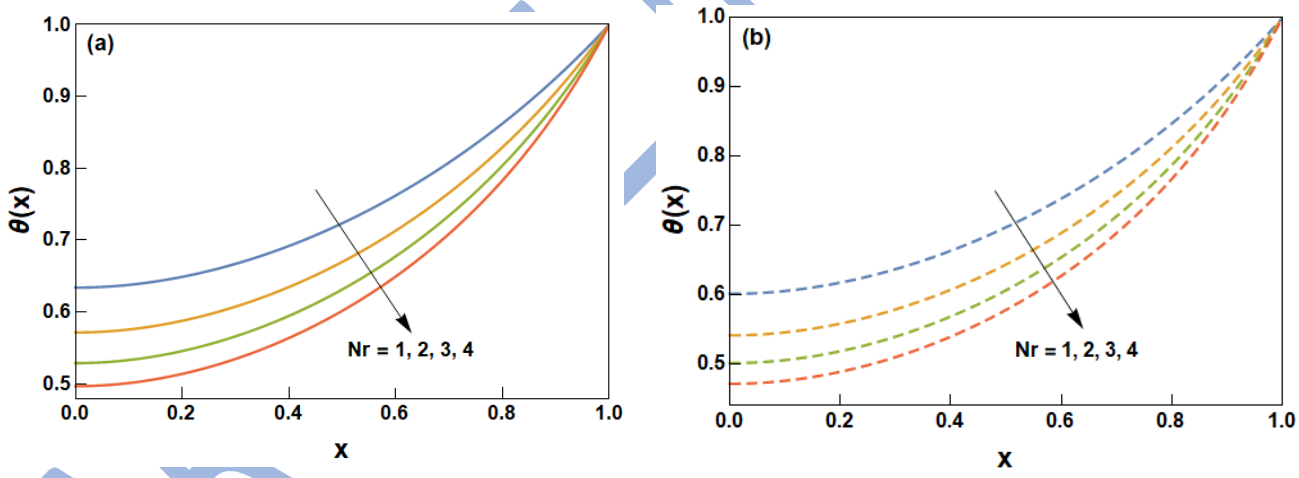


Fig. 5. Investigation of the effect of parameter Nr on $\theta(X)$ for (a) linear and (b) nonlinear thermal conductivity. ($C = 0$, $Nc = 1$, $Nt = 0.1$, $Pe = 1$, $Q = 0$, $n = 0$, $\gamma = 0.3$, $\beta = 0.3$, $\alpha = 0.1$, $m = 0$).

Fig. 5 indicates that as the radiation–conduction parameter (Nr)increases, the fin exhibits a lower dimensionless temperature profile. This behavior arises because a larger Nr corresponds to stronger radiative heat dissipation from the fin, which reduces its nondimensional temperature.

Figs. 6(a) and 6(b) show how the Péclet number (Pe) influences the fin's nondimensional temperature profile under both linear and nonlinear thermal-conductivity conditions.

AN - IN PRESS

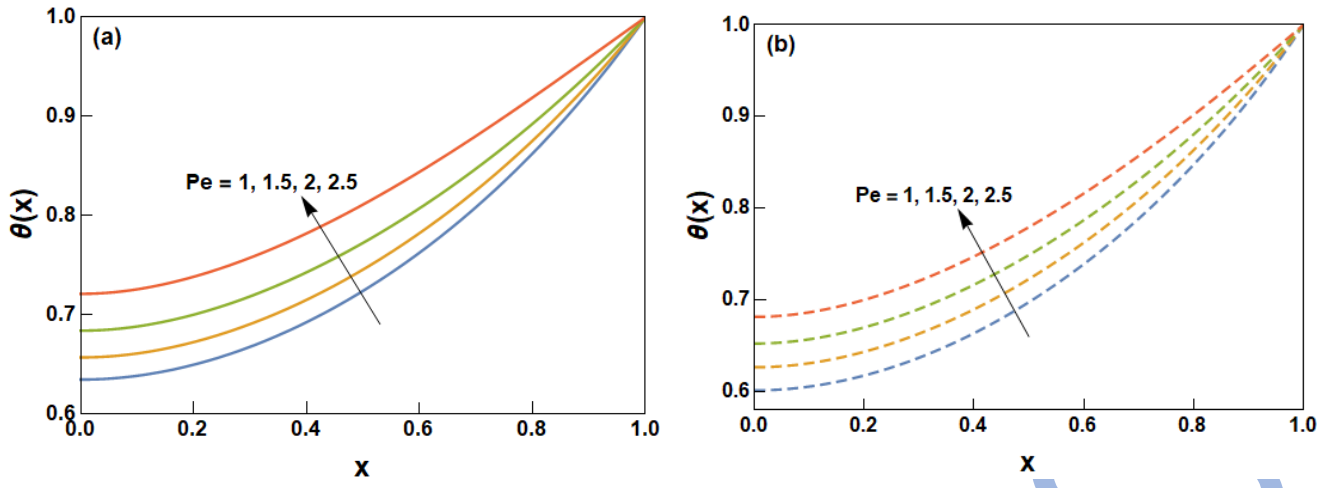


Fig. 6. Investigation of the effect of parameter Pe on $\theta(X)$ for (a) linear and (b) nonlinear thermal conductivity. ($C = 0$, $Nc = 1$, $Nt = 0.1$, $Nr = 1$, $Q = 0$, $n = 0$, $\gamma = 0.3$, $\beta = 0.3$, $\alpha = 0.1$, $m = 0$).

As illustrated in Fig. 6, larger values of the Péclet number (Pe) cause the fin's dimensionless temperature to increase. This parameter reflects the relative importance of convective heat transport compared with thermal diffusion inside the fin. When Perises, convection becomes more dominant, leaving less opportunity for heat exchange between the fin surface and the surrounding fluid; as a result, the fin maintains a higher nondimensional temperature.

As can be seen in Fig. 6, the fin dimensionless temperature increases as the Péclet number (Pe) Peincreases. The Péclet number represents the relative importance of convection associated with the fin motion compared with thermal diffusion within the fin. With increasing Pe, convective transport along the direction of fin motion becomes more dominant than thermal diffusion. Under the conditions considered in this study, this shift in the balance between convection and diffusion results in greater retention of thermal energy within the fin and, consequently, a higher dimensionless temperature.

The influence of the internal heat generation parameter (Q) on the fin's nondimensional temperature profile is presented in Figs. 7(a) and 7(b).

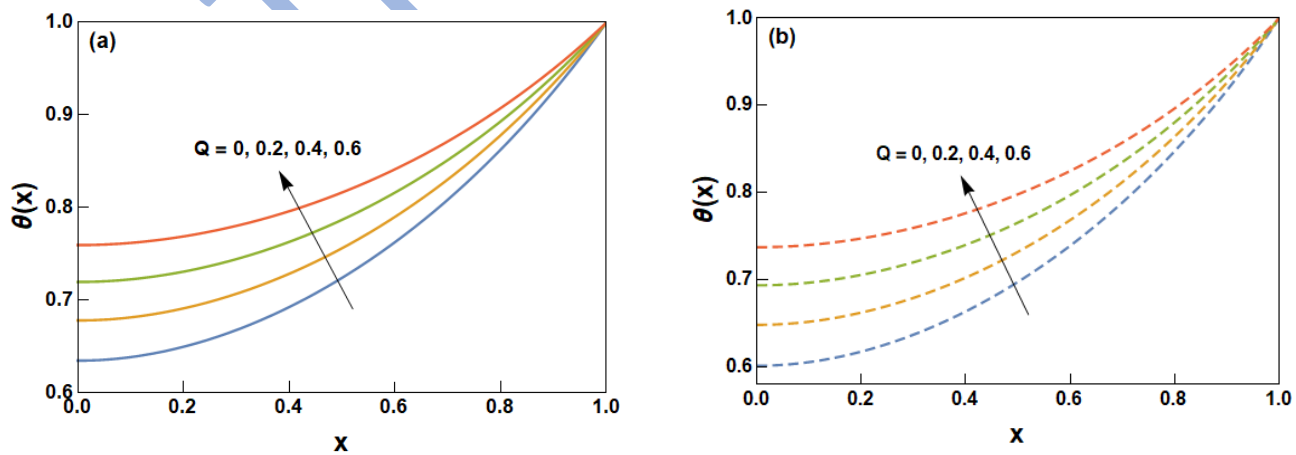


Fig. 7. Investigation of the effect of parameter Q on $\theta(X)$ for (a) linear and (b) nonlinear thermal conductivity. ($C = 0$, $Nc = 1$, $Nt = 0.1$, $Nr = 1$, $Pe = 1$, $Q = 0.1$, $n = 0$, $\gamma = 0.3$, $\beta = 0.3$, $\alpha = 0.1$, $m = 0$).

TICLE IN PRESS

As shown in Fig. 7, the fin dimensionless temperature increases with increasing heat-generation parameter (Q). Physically, a larger Q enhances the rate of internal heat generation within the fin, thereby imposing a higher thermal load inside the fin. Accordingly, under the conditions considered, the fin dimensionless temperature increases.

Fig. 8 illustrates the variation of fin efficiency with respect to the convection–conduction parameter (*Nc*) for different values of the radiation–conduction parameter (*Nr*). Fig. 8(a) corresponds to the case with linear thermal conductivity, while Fig. 8(b) represents the case with nonlinear thermal conductivity.

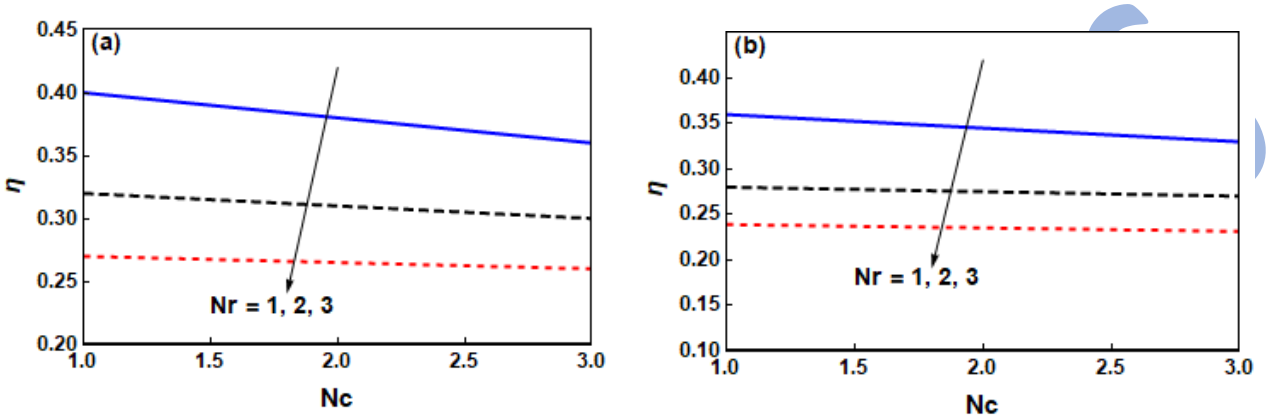


Fig. 8. Variation of fin efficiency with the convection–conduction parameter (*Nc*) for different values of the radiation–conduction parameter (*Nr*). ($C = 0.1$, $Nt = 0.1$, $Pe = 0.5$, $Q = 0.1$, $n = 0$, $\gamma = 0.3$, $\beta = 0.3$, $\alpha = 0.1$, $m = 0$).

Fig. 8 shows that when the parameters governing convection–conduction (*Nc*) and radiation–conduction (*Nr*) become larger, the overall thermal performance of the fin declines. This behavior occurs because greater *Nc* and *Nr* promote stronger heat removal through convection and radiation, leading to a drop in the nondimensional temperature and, as a result, a decrease in fin efficiency. The results indicate that, on average, the fin efficiency in the linear conduction case is approximately 14 percent higher than that in the nonlinear conduction case.

Fig. 9 illustrates the fin efficiency as a function of the temperature ratio parameter (*Nt*) for various values of the fin aspect ratio (*C*). Fig. 9(a) corresponds to the linear thermal conductivity case, while Fig. 9(b) represents the nonlinear thermal conductivity scenario.

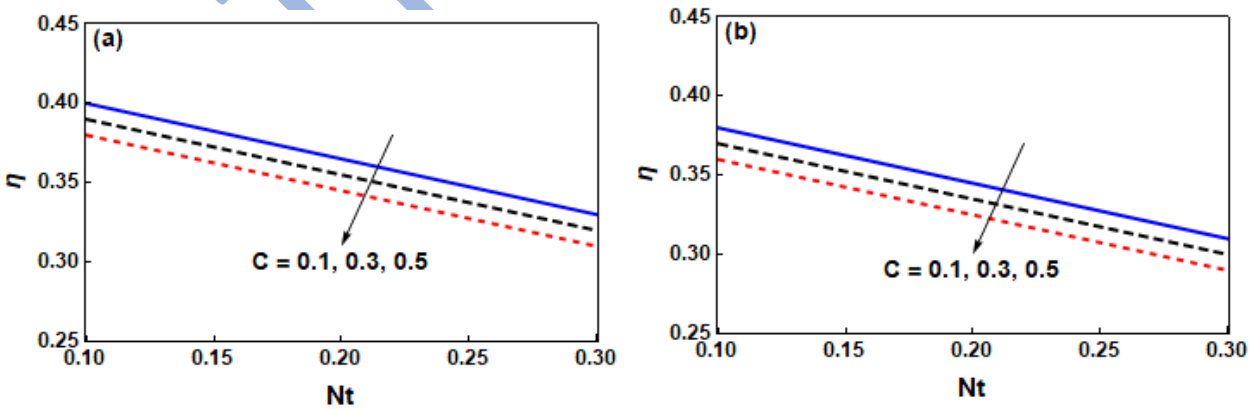


Fig. 9. Variation of fin efficiency with the temperature ratio parameter (*Nt*) for different values of the fin aspect ratio (*C*). ($Nc = 1$, $Nr = 1$, $Pe = 0.25$, $Q = 0.1$, $n = 0$, $\gamma = 0.3$, $\beta = 0.1$, $\alpha = 0.1$, $m = 0$).

Fig. 9 indicates that increasing the temperature-ratio parameter (*Nt*) as well as the fin aspect ratio (*C*) diminishes the thermal performance of the fin. A larger aspect ratio expands the effective lateral area of the fin, whereas a rise in *Nt*

strengthens the convective heat-transfer coefficient. The simultaneous influence of the increased surface area and intensified convection lowers the fin's dimensionless temperature, which eventually reduces its overall efficiency. Furthermore, the results indicate that, on average, the fin efficiency in the linear conduction case is approximately 8 percent higher than that in the nonlinear conduction case.

Fig. 10 illustrates the fin efficiency as a function of the heat source parameter (Q) for various values of the Péclet number (Pe). Fig. 10(a) corresponds to the linear thermal conductivity case, while Fig. 10(b) represents the nonlinear thermal conductivity scenario.

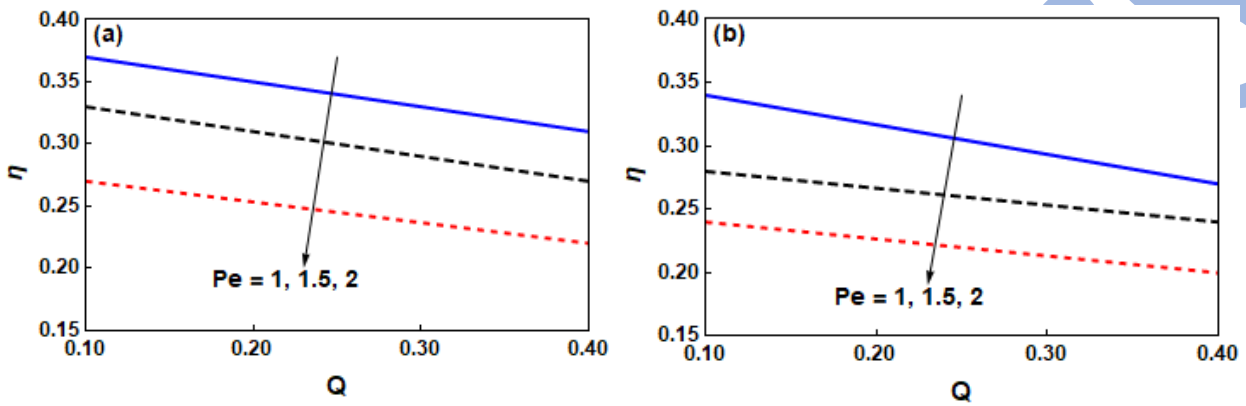


Fig. 10. Variation of fin efficiency with the heat source parameter (Q) for different values of the Péclet number (Pe). ($C = 0$, $Nc = 1$, $Nt = 0.1$, $Nr = 1$, $n = 0$, $\gamma = 0.3$, $\beta = 0.1$, $\alpha = 0.1$, $m = 0$).

According to the trends illustrated in Fig. 10, increasing both the Péclet number and the heat-source parameter leads to a reduction in fin efficiency. A higher Péclet number intensifies heat transfer inside the fin, while a larger value of the heat-source parameter enhances internal thermal energy generation. As a result, the fin's nondimensional temperature rises and gradually approaches the temperature at the fin base, which weakens the temperature gradient along the fin. This diminished temperature gradient ultimately contributes to a lower fin efficiency. Furthermore, the results indicate that, on average, the fin efficiency in the linear conduction case is approximately 8 percent higher than that in the nonlinear conduction case.

From the above Figs, it can be seen that the dimensionless temperature and fin efficiency in the linear thermal conductivity case are higher than in the nonlinear thermal conductivity case.

The results of the present study can be used in the design and optimization of heat-transfer systems based on moving fins, particularly in the cooling of electronic devices, heat exchangers, and thermal management systems. In particular, the parametric results of this research may be useful for selecting suitable conditions to improve the thermal performance of these systems.

8. Conclusion

The concluding remarks of the present study are briefly summarized as follows:

- The HPM method proves to be an efficient and effective approach for solving nonlinear equations, such as the nonlinear ordinary differential equation governing the temperature distribution of a moving trapezoidal fin.

ARTICLE IN PRESS

- From a convergence standpoint, the HPM provides increasingly accurate successive approximations to the solution as the number of expansion terms increases. In the present problem, using the first five terms of the HPM expansion has yielded results that are very close to the numerical RKF-45 solution.
- The HPM results of the present study show good agreement with the semi-analytical and numerical results reported in previous research.
- Increasing the fin blade ratio, convective-conductive parameter, temperature ratio parameter, and radiation-conductive parameter decreases the dimensionless fin temperature.
- Increasing the Peclet number and the heat source parameter leads to an increase in the dimensionless fin temperature.
- Increasing the fin blade ratio, convection-conduction parameter, temperature ratio parameter, radiation-conduction parameter, Peclet number, and heat source parameter decreases the fin efficiency.
- The dimensionless fin temperature and fin efficiency are slightly higher for the linear thermal conductivity case compared to the nonlinear thermal conductivity case.
- The results of the present study can be applied to the design and optimization of heat-transfer systems based on moving fins, particularly in applications related to the cooling of electronic equipment, heat exchangers, and thermal management systems.

ARTICLE IN PRESS

Nomenclature

Q	Dimensionless internal heat generation parameter
U	Velocity of the fin (m s^{-1})
Nc	Convection–conduction parameter
T_b	Base temperature of fin (K)
$t(x)$	Local semi-fin thickness (m)
σ	Stefan–Boltzmann constant (W m^{-2} K^{-4})
κ	Temperature-dependent thermal conductivity coefficient (K^{-1})
η	Efficiency of the fin
T_a	Ambient temperature (K)
Nt	Temperature ratio parameter
C_p	Specific heat of the fin material (J kg^{-1} K^{-1})
Nr	Radiation–conduction parameter
ρ	Density of the fin material (kg m^{-3})
γ	Dimensionless variable internal heat generation parameter
β	Variable thermal conductivity parameter (dimensionless)
δ^*	Semi-offset (m)
W	Width of the fin (m)
κ_a	Thermal conductivity at ambient temperature (W m^{-1} K^{-1})
$k^*(T)$	Thermal conductivity (W m^{-1} K^{-1})
h^*	Convective heat transfer coefficient (W m^{-2} K^{-1})
θ	Non-dimensional temperature
x	Fin axial distance (m)
t_b	Thickness of the fin at the base (m)
L	Length of the fin (m)
$q(T)$	Uniform internal heat generation (W m^{-3})
h_b	Heat transfer coefficient at the base of the fin (W m^{-2} K^{-1})
X	Dimensionless length fin
Pe	Peclet number
T	Temperature (K)
$\varepsilon^*(T)$	Emissivity
C	Fin taper ratio
α	Emissivity variation parameter
ε^*	Temperature-dependence coefficient of emissivity (K^{-1})
ε_s	Radiation heat transfer coefficient

ARTICLE IN PRESS

References

[1] Torabi, M., Yaghoobi, H., Aziz, A., 2012. Analytical solution for convective–radiative continuously moving fin with temperature-dependent thermal conductivity, International Journal of Thermophysics, 33, 924-941. http://dx.doi.org/10.1007/s10765-012-1179-z

[2] Sun, Y.S., Xu, J.L., 2015. Thermal performance of continuously moving radiative–convective fin of complex cross-section with multiple nonlinearities, International Communications in Heat and Mass Transfer, 63, 23-34. http://dx.doi.org/10.1016/j.icheatmasstransfer.2015.01.011

[3] Roy, P.K., Mallick, A., 2016. Thermal analysis of straight rectangular fin using homotopy perturbation method, Alexandria Engineering Journal, 55, 2269-2277. http://dx.doi.org/10.1016/j.aej.2016.05.020

[4] Sobamowo, M.G., 2017. Analysis of convective longitudinal fin with temperature-dependent thermal conductivity and internal heat generation, Alexandria Engineering Journal, 56, 1-11. http://dx.doi.org/10.1016/j.aej.2016.11.001

[5] Patel, T., Meher, R., 2017. Thermal analysis of porous fin with uniform magnetic field using Adomian decomposition Sumudu transform method, Nonlinear Engineering, 6(3), 191-200. http://dx.doi.org/10.1515/nleng-2017-0021

[6] Oguntala, G., Abd-Alhameed, R., Ngala, M., 2019. Transient thermal analysis and optimization of convective-radiative porous fin under the influence of magnetic field for efficient microprocessor cooling, International Journal of Thermal Sciences, 145, 106019. http://dx.doi.org/10.1016/j.ijthermalsci.2018.10.026

[7] Das, R., Kundu, B., 2020. Estimating magnetic field strength in a porous fin from a surface temperature response, Electronics Letters, 56(19), 1011-1013. http://dx.doi.org/10.1049/el.2020.1655

[8] Jayaprakash, M.C., Alzahrani, H.A.H., Sowmya, G., Varun Kumar, R.S., Malik, M.Y., Alsaiari, A., Prasannakumara, B.C., 2021. Thermal distribution through a moving longitudinal trapezoidal fin with variable temperature-dependent thermal properties using DTM-Pade approximant, Case Studies in Thermal Engineering, 28, 101697. http://dx.doi.org/10.1016/j.csite.2021.101697

[9] Ud Din, Z., Ali, A., De la Sen, M., Zaman, G., 2022. Entropy generation from convective–radiative moving exponential porous fins with variable thermal conductivity and internal heat generations, Scientific Reports, 12, 1791. https://doi.org/10.1038/s41598-022-05507-1
[10] Xu, Y.J., Hashemi, M.S., 2023. Exact solutions for porous fins under a uniform magnetic field: A novel reduction method, Case Studies in Thermal Engineering, 45, 103013. http://dx.doi.org/10.1016/j.csite.2023.103013
[11] Riasat, S., Bilal, S., Alshehery, S., Khan, N., Ali, M.R., Hendy, A.S., 2024. Unsteady thermal efficiency and temperature isotherms of an inclined radiative porous concave parabolic tapered fin: An application of design of tapered fin featuring, Case Studies in Thermal Engineering, 63, 105318. http://dx.doi.org/10.1016/j.csite.2024.105318
[12] Pavithra, C.G., Gireesha, B.J., 2024. Heat transfer in a wet porous moving inclined longitudinal fin exposed to convection and radiation in the presence of shape-dependent hybrid nanofluid: Adomian decomposition Sumudu transformation approach, Journal of Molecular Liquids, 393, 123582. http://dx.doi.org/10.1016/j.jmliq.2023.123582
[13] Pavan Kumar, P.L., Gireesha, B.J., Venkatesh, P., Keerthi, M.L., 2025. Comparative analysis of transient thermal behaviour and efficiency in longitudinal metal porous fin with combined heat and mass transfer under dehumidification conditions, Applied Thermal Engineering, 261, 125069. http://dx.doi.org/10.1016/j.applthermaleng.2024.125069
[14] Ahmad, I., Zahid, H., Zahoor Raja, M.A., Ilyas, H., Mohayyuddin, Z., 2025. Use of Levenberg-Marquardt networks for optimization of thermal dispersion in moving triangular porous fin, International Journal of Thermal Sciences, 210, 109613. http://dx.doi.org/10.1016/j.ijthermalsci.2024.109613
[15] Singh, S., Kaur, P., Kumar, D., Rai, K.N., 2025. Wavelet collocation solution for fully wet semi-spherical porous fin, Partial Differential Equations in Applied Mathematics, 13, 101012. http://dx.doi.org/10.1016/j.padiff.2024.101012
[16] Khani, F., Aziz, A., 2010. Thermal analysis of a longitudinal trapezoidal fin with temperature-dependent thermal conductivity and heat transfer coefficient, Communications in Nonlinear Science and Numerical Simulation, 15(3), 590-601. http://dx.doi.org/10.1016/j.cnsns.2009.04.028
[17] Das, R., 2016. Estimation of feasible materials and thermal conditions in a trapezoidal fin using genetic algorithm, Proceedings of the Institution of Mechanical Engineers, Part G: Journal of Aerospace Engineering, 230(13), 2356-2368. http://dx.doi.org/10.1177/0954410015623975
[18] Nabati, M., Salehi, G.H., Taherifar, S., 2023. Numerical solution for a porous fin thermal performance problem by application of Sinc collocation method, Mathematical Methods in the Applied Sciences, 46(10), 11373-11391. http://dx.doi.org/10.1002/mma.7740
[19] Roy, P.K., Mallick, A., Mondal, H., Sibanda, P., 2018. A modified decomposition solution of triangular moving fin with multiple variable thermal properties, Arabian Journal for Science and Engineering, 43(3), 1485-1497. http://dx.doi.org/10.1007/s13369-017-2983-3
[20] He, J.H., 1999. Homotopy perturbation technique, Computer Methods in Applied Mechanics and Engineering, 178, 257-262. http://dx.doi.org/10.1016/S0045-7825(99)00018-3
[21] He, J.H., 2000. A coupling method of a homotopy technique and a perturbation technique for non-linear problems, International Journal of Non-Linear Mechanics, 35(1), 37-43. http://dx.doi.org/10.1016/S0020-7462(00)00018-7
[22] Turkyilmazoglu, M., 2018. A reliable convergent Adomian decomposition method for heat transfer through extended surfaces, International Journal of Numerical Methods for Heat & Fluid Flow, 28(11), 2551-2566. http://dx.doi.org/10.1108/HFF-01-2018-0003
[23] Roy, P.K., Mallick, A., 2016. Thermal analysis of straight rectangular fin using homotopy perturbation method, Alexandria Engineering Journal, 55(3), 2269-2277. http://dx.doi.org/10.1016/j.aej.2016.05.020

